EXPERIMENTAL AND NUMERICAL INVESTIGATIONS OF THE WAKE VORTEX SYSTEM OF A DELTA-CANARD-CONFIGURATION

Jan-Ulrich Klar, Christian Breitsamter, and Nikolaus Adams
Institute of Aerodynamics, Technische Universität München
Boltzmannstrasse 15, D-85748 Garching, Germany

Keywords: *Unsteady Aerodynamics, High Agility Aircraft, Wake Penetration, Wake Vortex system*

Abstract

The presented investigation includes a combined experimental-numerical approach to quantify the wake vortex system of a high-agility aircraft from the near field up to the far field. Detailed near field data are obtained by low-speed wind tunnel tests on a delta-canard configuration of 1:15 scale. The measurements are performed at several angles of attack applying advanced hot-wire anemometry. For a wake distance of up to 16 wing spans, mean and turbulent velocity fields are measured. The upstream data are used to initialize Implicit Large-Eddy Simulations (ILES) aimed to compute the velocity fields of the wake vortex system over a wake distance of up to 50 spans. Here, a validation case is shown comparing measured and calculated wake data over a distance from 4 to 16 spans, with the ILES computations initialized by the measured quantities at a position of 2 wing spans. Compared to the experimental data, the numerical results show the expected lateral and vertical movement of the wake vortex system due to the interaction of the single vortices. The distributions of axial vorticity, cross flow velocities and turbulence intensities match well with the experimental data. In addition, the dissipation process can be observed, resulting in a reduction of circulation. In context of this study, the measured and computed velocity fields will be used to determine unsteady aerodynamic loads acting on a fighter aircraft encountering the wake. This is of great importance as wake induction may result in critical structural dynamic loads.

Nomenclature

$\AA R$	=	aspect ratio
A	=	area of the measured cross flow plane, m^2
b	=	wing span, m
l_μ	=	wing mean aerodynamic chord, m
Re_{l_μ}	=	Reynolds number, $U_\infty l_\mu/\nu$
U_∞	=	freestream velocity, m/s
u, v, w	=	axial, lateral, and vertical velocities, m/s
$\overline{u}$, $\overline{v}$, $\overline{w}$	=	mean axial, lateral, and vertical velocities, m/s
u', v', w'	=	fluctuation part of u, v, and w, m/s
x, y, z	=	coordinates in x, y, and z directions, m
x^*	=	nondimensional distance in x direction, x/b
y^*, z^*	=	nondimensional distances in y and z direction, $2y/b$, $2z/b$
α	=	aircraft angle of attack, deg

ν = kinematic viscosity, m^2/s
ξ = nondimensional axial vorticity, $\overline{\omega}_x b/(2U_\infty)$
ρ = density, kg/m^3
$\overline{\omega}_x$ = mean axial vorticity component, $(d\overline{w}/dy - d\overline{v}/dz)$, 1/s
Γ_0 = root circulation, $\iint \overline{\omega}_x(y,z)dA$, m^2/s
f = frequency, Hz
u_{rms} = axial turbulence intensity, $\sqrt{\overline{u'^2}}$, m/s
v_{rms} = lateral turbulence intensity, $\sqrt{\overline{v'^2}}$, m/s
w_{rms} = vertical turbulence intensity, $\sqrt{\overline{w'^2}}$, m/s

1 Introduction

Structural dynamic loads of civil and military aircraft due to maximum velocities and velocity fluctuations associated with wake vortex systems are not sufficiently investigated [1]. Although, comprehensive wake vortex investigations have been performed, they are mainly aimed on wake vortex characterisation and control and safety issues related to wake vortex encounter [2-7]. In this context, reducing separation distances while maintaining the safety standards may help to increase the capacities on major airports. In contrast to civil aviation, high-agility aircraft have to cross or to fly in the wake of a preceding aircraft under certain circumstances. The scenarios include, for example, formation flight, air refueling and combat maneuvers. Conducted flight tests show a strong dynamic response of the elastic structure, which indicates critical loads acting on the aircraft [1]. The total aerodynamic load on an aircraft penetrating the wake results from the mean velocity distribution, the velocity fluctuations and the response of the elastic structure. Due to the relative movement and the partial large distance between the aircraft, experimental and numerical investigations covering the whole problem can hardly be performed. For this reason the problem is broken down to a crossing and a flying in the wake problem. First assumes a difference in the heading angle of the two aircraft. If it is big enough the following plane will only remain for a limited time in the wake. If the mean velocities in the wake are known the loads which occur during crossing could be computed following the strategy of the discrete gust problem [8-12]. Velocity fluctuations in the wake may be considered based on measured or calculated turbulence intensities. In the following it will be called the "discrete" wake problem. To calculate the dynamic response of an aircraft that flies over a longer time in the wake the problem is similar to the "continuous" gust problem [8-12]. In contrast, the mean velocity of the wake can be neglected if there is no or only a minor difference of the heading angle. Using the frequency and amplitude of the velocity fluctuations in the wake the resulting unsteady loads on an aircraft flying in the wake could be calculated based on Potential [13] or Euler methods [14]. Furthermore, the mentioned loads cause an excitation of the elastic aircraft. These structural vibrations lead to unsteady aerodynamic loads as well.
A determination of the unsteady aerodynamic loads requires detailed information of the velocity distribution in the wake. For this purpose Large-Eddy Simulations (LES) of the wake vortex system are conducted [15]. To provide detailed and precise flowfield data the LES calculations are initialized with experimentally obtained near field quantities of the wake generating aircraft. The necessary velocity fields are measured using advanced hot-wire anemometry. These quantities serve also as validation data considering cross flow stations located further downstream.

2 Experimental Investigation

The necessary data to initialize the numerical simulations include mean velocities and turbulence intensities. Therefore, hot-wire anemometry as measurement technique which is able to resolve the temporal flow-field at a high sampling rate is applied [16]. Experimental investigations of the wake vortex system are conducted in the wind

tunnel facility C of the Institute of Aerodynamics at the Technische Universität München. A 1:15 scaled detailed full-model of a delta-canard configuration is investigated (Fig. 1) serving as the wake generating aircraft.

Fig. 1 Delta-canard configuration mounted in the test section of wind tunnel C

The model has a wing span of 0.740 m ($\mathcal{R}$ = 2.45), a wing mean aerodynamic chord of 0.360 m and a wing leading edge sweep of 50 deg. The wind tunnel has a long-range test section which is 21 m in length, permitting theoretically the investigation of a wake distance up tp 19 spans downstream of the model. The cross section of 1.8 m x 2.7 m reduces wall interferences to an acceptable magnitude. A quadruple-wire probe operated by a multi channel constant-temperature anemometer system is used to measure the time series of axial, lateral and vertical velocities. The wires have a diameter of 5 μm and are arranged perpendicular to each other to achieve best angular resolution. An additional temperature probe is employed to correct anemometer output voltages if ambient flow temperature varies. A sampling rate of 3000 Hz (Nyquist frequency 1500 Hz) and a sampling time of 6.4 s has been chosen. The sampling time corresponds to 19200 values per survey point.
All of the investigations are performed at a free stream velocity of U_∞ = 25 m/s, corresponding to a Reynolds number of $Re_{l_\mu} = 5\,x\,10^5$. As wing reference point, from which the downstream position of the measured plane is determined, the wing tip trailing edge at an angle of attack of $\alpha = 0.0$ deg is chosen. Referring to the balance reference point of the model as the center of rotation to adjust the angle of attack, all downstream positions can be clearly identified. A three-axis traversing system is used to position the hot-wire probe in the test section during the measurements. The vortex wake is captured at cross flow planes orientated perpendicularly to the free stream direction at distances x* = x/b = 0.5, 1.0, 2.0, 4.0, 8.0, 12.0 and 16.0 for the angle of attack of $\alpha = 8$ deg. Due to the increasing induced downwash and the associated descent the wake at higher angles of attack, namely $\alpha = 15$ (Fig. 2) and 20 deg, is only investigated to x* = 12.0 and x* = 8.0, respectively, cf. Table 1.

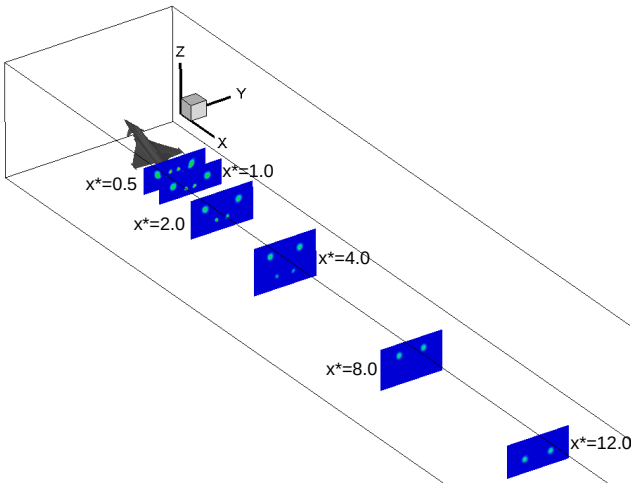

Fig. 2 Measured cross flow planes at x* = x/b = 0.5, 1.0, 2.0, 4.0, 8.0, and 12.0 for $\alpha = 15$ deg

The characteristics of the flow around an aircraft with low aspect ratio and high wing sweep are presented in Figs. 3 and 4.
The wake of the investigated delta-canard-configuration is influenced by vortices emanating from the wing, the canard and the fuselage. The wing and canard flow separates already at the leading edges for small angles of attack. The 3-dimensional boundary layer forms a wing leading

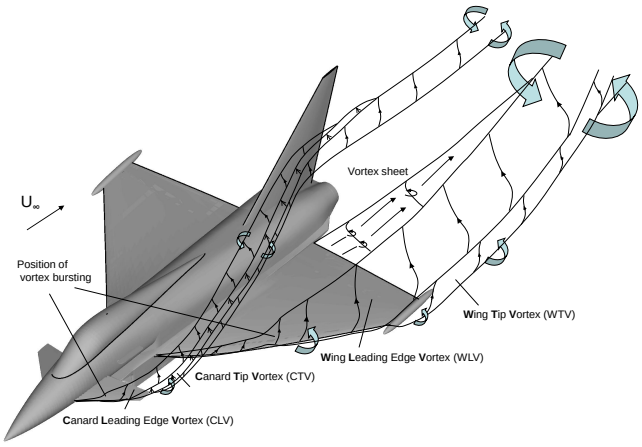

Fig. 3 Schematic representation of the vortex system of the delta-canard configuration.

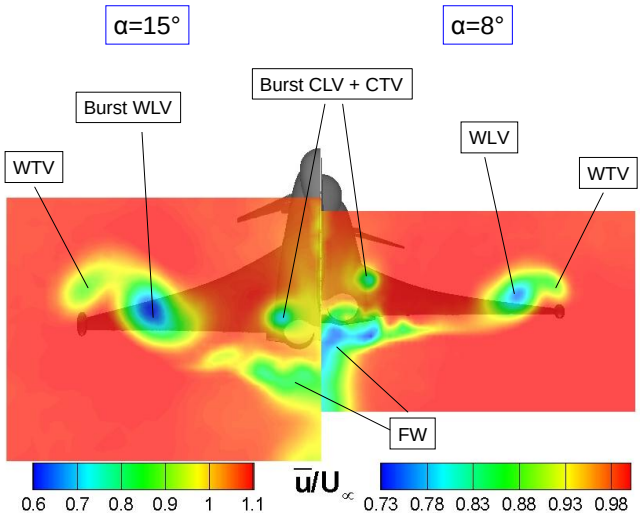

Fig. 4 Nondimensional axial velocity distributions $\bar{u}/U_\infty$ at x* = x/b = 0.5 for $\alpha = 8$ and 15 deg.

WLV Wing leading edge vortex

WTV Wing tip vortex

CLV Canard leading edge vortex

CTV Canard tip vortex

FW Fuselage wake

		Angle of attack, α		
		8 deg	15 deg	20 deg
Downstream position, x*	0.5	X	X	X
	1.0	X	X	X
	2.0	X	X	X
	4.0	X	X	X
	8.0	X	X	X
	12.0	X	X	
	16.0	X		

Table 1 Position of measured cross flow planes

edge vortex (WLV) and a canard leading edge vortex (CLV) [17]. The wing tip vortex (WTV) can be identified in the most upstream measured cross flow planes but then rolls up into the WLV. Similar counts for the canard tip vortex (CTV) with the difference that the roll-up process is already finished before reaching the trailing edge of the wing. As the main interest is on the wake further downstream the term WLV includes the WTV and the term CLV the CTV in the following discussions.

3 Numerical simulation of the wake vortex system

To catch the spatial and temporal development of the wake far downstream the use of an appropriate numerical method is necessary. The experimental investigations showed the wake vortex system is accompanied by unsteady turbulent flow with a broad range of spatial and temporal scales. For that kind of flows only Large Eddy Simulations (LES) are able to obtain sufficient accurate results by justifiable costs. The numerical code uses implicit modeling for the sub grid scales (SGS) which leads to the notation Implicit Large Eddy Simulation (ILES). The truncation error of the discretization of the convective terms acts as a SGS model which is therefore implicit to the discretization. The used code INCA was developed at the Institute of Aerodynamics (AER) at the Technische Universität München (TUM). The implementation of ILES is here the Adaptive Local Deconvolution Method (ALDM) [15].

3.1 Grid generation and numerical setup

The ILES flow solver INCA uses a Cartesian grid method with adaptive mesh refinement by zonal embedding. All calculations are performed on the High Performance Computer HLRB2 on the Leibniz-Rechenzentrum. The domain is split into a number of sub-blocks which are then calculated each on an own processor. For effective calculations, all of these blocks should consist approximately of the same number of cells. For that purpose a grid generator is programmed aimed to optimize the dimensions of the blocks to fulfill the mentioned requirements. In Fig. 5, the flowfield domain divided in blocks for the "validation case" is shown. This case refers to the delta-canard wake at α = 8 deg taking into account the wind tunnel test section dimensions as domain boundaries for the ILES calculation. The ceiling, the floor and the walls of the wind tunnel are modelled as slip walls. At the outflow of the domain a constant static pressure condition is set.

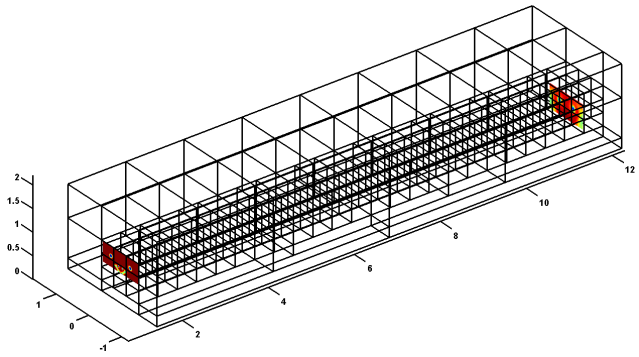

Fig. 5 Flowfield domain for the validation calculations for α=8 deg

The simulation under free flight conditions requires an enlargement of the lateral and vertical dimensions to reduce the influence of the domain boundaries. In Fig. 6, the domain for the free flight simulation for α = 8 deg is shown.
Outside the regions with high gradients the resolution of the numerical grid can be reduced. Therefore, the overall domain consists of three different mesh sizes which are listed in Table 2.

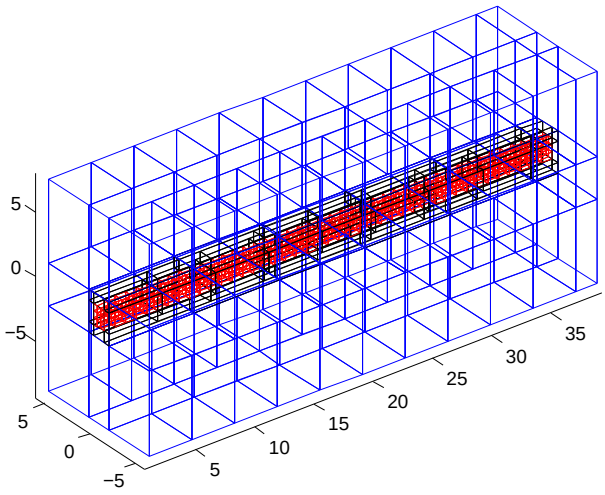

Fig. 6 Flowfield domain for the free flight calculations for α=8 deg

	Validation simulations		
	Free Flight simulations		
	fine	*middle*	*coarse*
Δx	50 mm	150 mm	450 mm
	$\Delta x/(b/2)$= 0,135	$\Delta x/(b/2)$= 0,4	$\Delta x/(b/2)$= 1,2
Δy	5 mm	15 mm	45 mm
	$\Delta y/(b/2)$= 0,0135	$\Delta y/(b/2)$= 0,04	$\Delta y/(b/2)$= 0,12
Δz	5 mm	15 mm	45 mm
	$\Delta z/(b/2)$= 0,0135	$\Delta z/(b/2)$= 0,04	$\Delta z/(b/2)$= 0,12
Δt	$\approx$ 0,0001 s		

Table 2 Chosen grid resolution and timestep for the validation case and the free flight simulations

The red colored blocks have the finest, the black colored blocks a medium and the blue colored blocks the coarsest resolution. The time step Δt is adjusted dynamically according to a Courant-Friedrichs-Lewy (CFL) limit depending on the mean velocity $\overline{u}$, the grid size and the kinematic viscosity ν [15]. With the chosen time step frequencies up to 5000 Hz can be resolved in the ILES computations. Fig. 7 shows an example of the spectral content of the axial velocity fluctuations measured at x* = 16.0 and α = 8 deg in the vortex center.

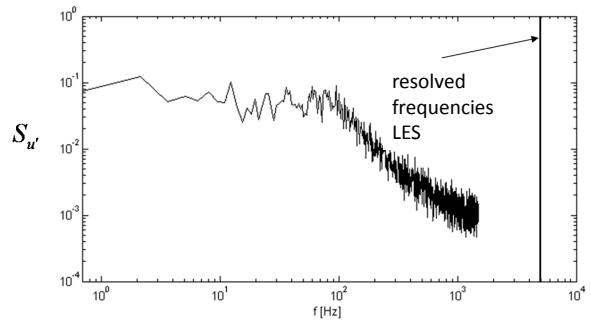

Fig. 7 Power spectral density of u' in the vortex center at x*=16.0 and α=8 deg

The low pass filter set at 1000 Hz due to the Nyquist criterion limits the experimental frequency range which is below the ILES resolved frequencies.
Free flight simulations include downstream positions which are not measured during the wind tunnel investigations. Therefore, information of the descent of the vortex system is missing. Accordingly, the vertical dimension of the high resolved grid region is unknown. This could be estimated by using the induced downwash of a potential vortex with:

$$w_{ind} = \frac{\Gamma_0}{2\pi \cdot 2y_{pv}} \tag{1}$$

The positon (y_{pv}, z_{pv}) of this vortex can be found by

$$\begin{aligned} y_{pv} &= \frac{1}{\Gamma_0} \iint y \cdot \overline{\omega}_x(y,z) dA \\ z_{pv} &= \frac{1}{\Gamma_0} \iint z \cdot \overline{\omega}_x(y,z) dA. \end{aligned} \tag{2}$$

The vorticity distribution of the most downstream located measurement position is used. Together with the known freestream velocity U_∞ and the axial dimension of the domain the vertical descent of the vortex system can be estimated.

3.2 Preparing experimental data to initialize ILES

Besides the advantage of the highly temporal resolution the hot-wire anemometry has a huge effort of time. Assuming symmetry of the model only one half of the wing span is measured. Further, only regions close to the vortex system are resolved. For initialisation of the numerical simulation a much bigger region has to be set in the inflow plane. Two different kinds of numerical simulations are performed. In the scope of validation calculations the objective is to reproduce the wind tunnel conditions as close as possible. In this case the ceiling, the walls and the floor of the wind tunnel are the boundaries of the simulation domain. Furthermore, the influence of the model mount has to be considered. The cross flow components $\overline{v}$ and $\overline{w}$ are not as easy to reconstruct as the velocity $\overline{u}$ and the turbulence intensities u_{rms}, v_{rms} and w_{rms}. The influence of the vortex system on the cross flow velocities is also present across the boundaries of the measured cross flow plane. In the outer regions the cross flow velocities of the vortex are modelled by a potential vortex. The velocity field induced by the calculated potential vortex is used to set the cross flow velocities in the not measured or mirrored regions (Fig. 8).
Thus, high gradients between the known and the reconstructed regions are avoided. Accordingly, the values for the vertical velocity $\overline{w}$ are determined. In contrast, the turbulence intensities u_{rms}, v_{rms} and w_{rms} are set to the test section minimum values for all unknown regions except the region between the ground and the measured and mirrored area. Here, the wake of the model mount is

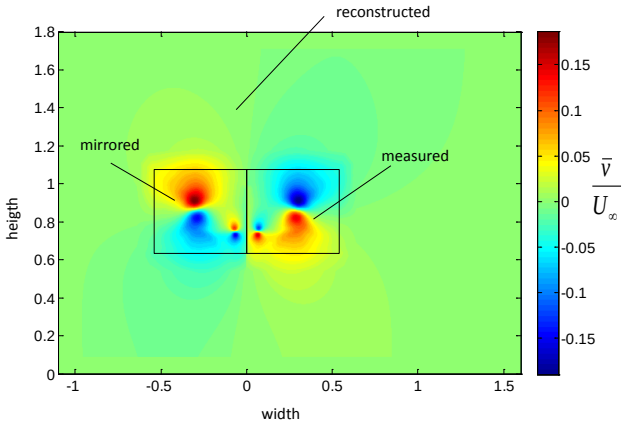

Fig. 8 Lateral velocity distribution $\bar{v}/U_\infty$ at the inflow plane for the validation calculations of the delta-canard wake vortex system at $\alpha = 8$ deg

considered by copying the values from the lowest measured grid line to the total unknown area.

4 Results and Discussion

The discussion is focused on the comparison between the experiment and the validation calculations. The major interst regarding the wake penetration is the spatial development of the wake vortex system and the velocity distribution, especially of the vertical component *w*. As given by Eq. 1 the sink speed of the vortex system depends on the lateral position and the circulation of the WLVs and the CLVs. Contour plots of the nondimensional axial vorticity ξ are shown for both the experiment and ILES at x* = 4.0, 8.0, 12.0, and 16.0 in Fig. 9.

At the downstream position x* = 4.0, the CLV and the WLV can be identified both in the experiment and in the ILES. A shear layer exists between the two vortices which indicates a circulation exchange. While the maximum vorticity values of the experiment and the ILES are nearly the same for the WLV this does not hold for the CLVs. In Fig. 10, the nondimensional circulation of the single vortices is plotted as function of the downstream distance x*.

In the experiment the CLV dissipates earlier as

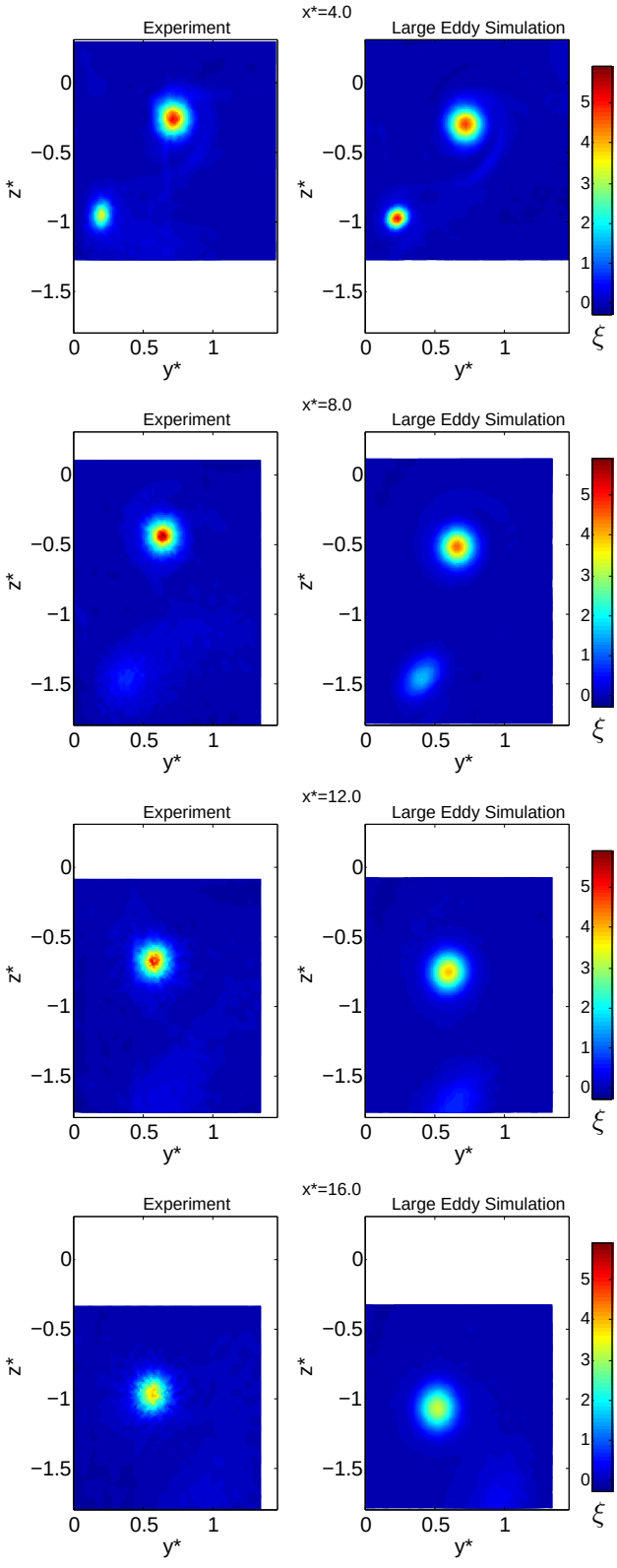

Fig. 9 Contour plots of nondimensional axial vorticity ξ at x* = 4.0, 8.0, 12.0, and 16.0 for $Re_{l_\mu} = 5x10^5$ and $\alpha = 8$ deg

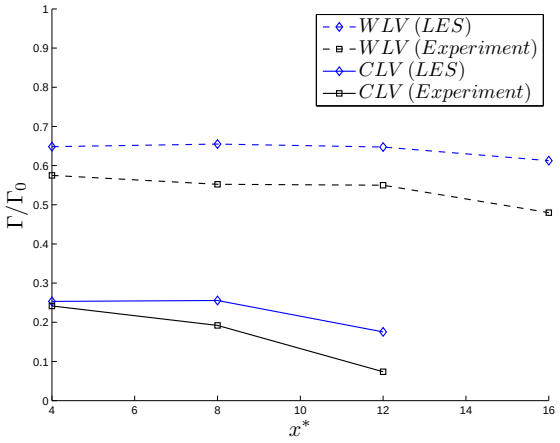

Fig. 10 Nondimensional circulation Γ/Γ_0 of the WLV and the CLV at x* = 4.0, 8.0, 12.0, and 16.0 for the experiment and the simulation

it does in the ILES. Due to the downwash close to the plane of symmetry the CLV sinks much faster than the WLV. Fig. 11 and Fig. 12 show the position of the WLVs and the CLVs in the x-z and y-z plane respectively.

The spatial development of the WLV and CLV in the y-z plane is similar in the experiment and the numerical simulation. Since the CLVs are located closer to the plane of symmetry, the vertical displacement is much higher as it is for the WLVs. The negativ curvature of the WLV in Fig. 11 indicates that the induced downwash increases with the downstream position. For an isolated vortex pair a decrease is to be expected due to dissipation effects and therefore an reduction of circulation. The lateral movement of the WLVs shown in Fig. 12 reduces the distance between the WLV pair, thus increasing the induced downwash. This influence could be seen in the nondimensional vertical velocity $\overline{w}/U_\infty$ shown in Fig. 13. Additionally, the nondimensional vertical velocity $\overline{w}/U_\infty$ ist plotted in a horizontal cut through the vortex center in Fig. 14.

In the ILES and the experiment the typical vertical velocity distribution for a trailing vortex pair is shown. Due to the fact that the lateral position is slightly different in the experiment and the ILES the maximum and minimum values vary because the same scale is chosen. This difference

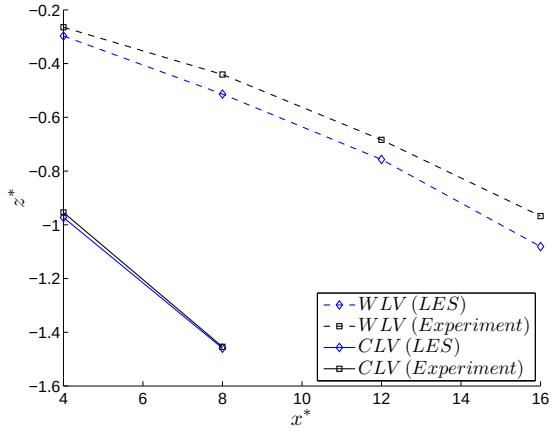

Fig. 11 Vertical position z^* of the WLV and the CLV for the experiment and the simulation

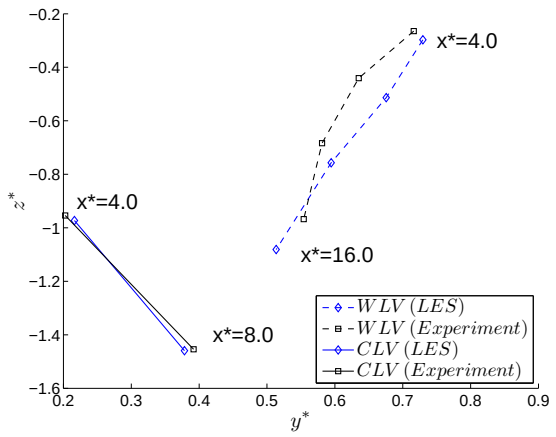

Fig. 12 Lateral position y^* of the WLV and the CLV for the experiment and the simulation

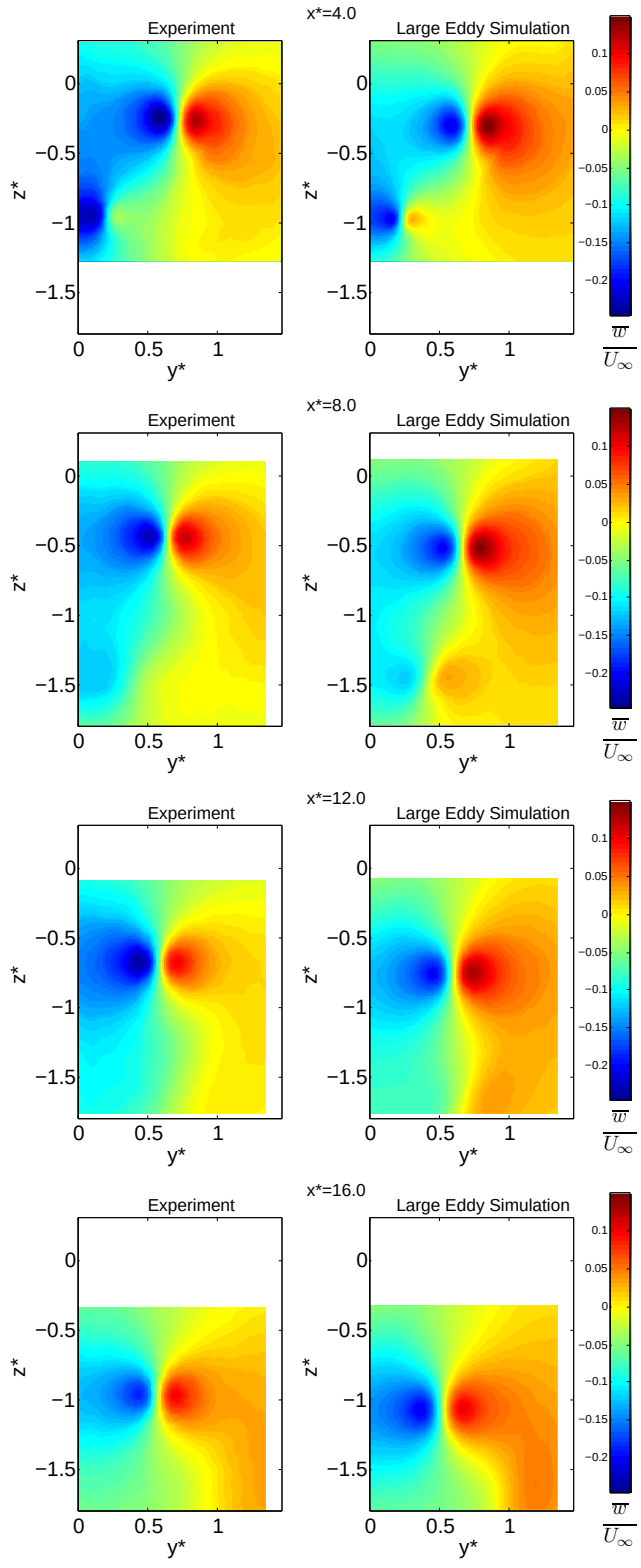

Fig. 13 Contour plots of nondimensional vertical velocity $\overline{w}/U_\infty$ at x* = 4.0, 8.0, 12.0, and 16.0 for $Re_{l_\mu} = 5x10^5$ and $\alpha = 8$ deg

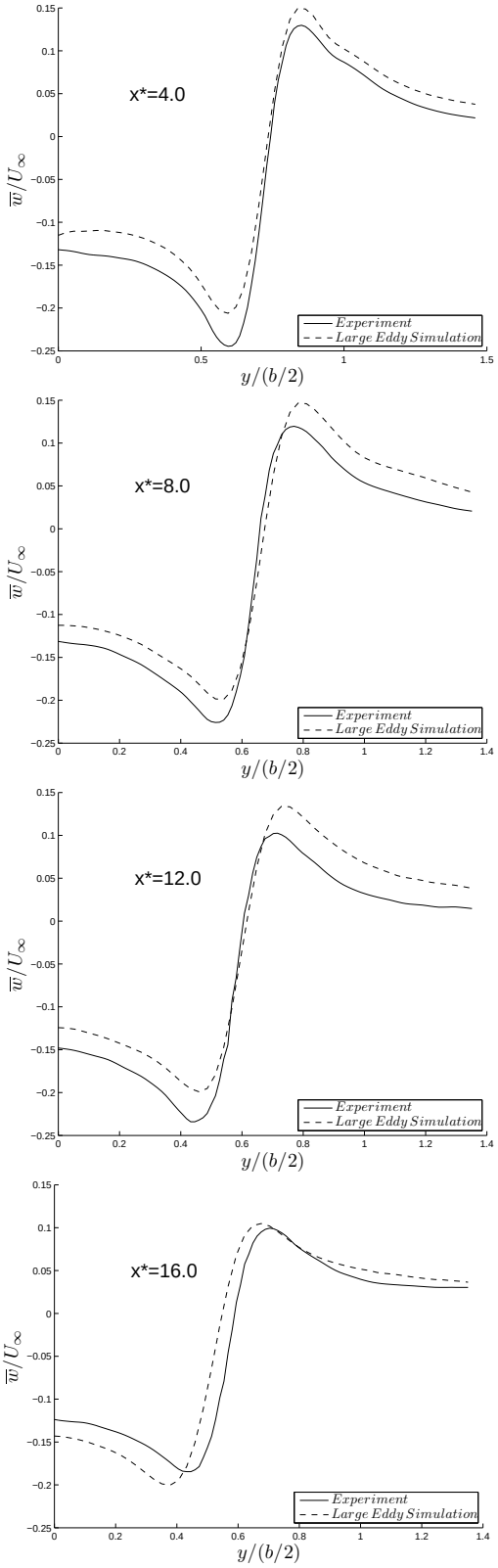

Fig. 14 Nondimensional vertical velocity $\overline{w}/U_\infty$ for a cut through the vortex center for $Re_{l_\mu} = 5x10^5$ and $\alpha = 8$ deg

can also be seen in Fig. 14. Close to the vortex center the velocity distribution is similar to the rotation of a rigid body. Due to high viscosity the velocity increases with the distance from the vortex center. Considering an aircraft which encounters the wake, the unsteady angle of attack is mainly defined by the vertical velocity fluctuations w'. To identify the regions of high vertical fluctuations Fig. 15 shows contour plots of the nondimensional vertical turbulence intensity w_{rms}/U_∞. To allow a direct comparison of the experiment and the numerical results, Fig. 16 shows the nondimensional vertical turbulence intensity w_{rms}/U_∞ for a horizontal cut through the vortex center.

In the most upstream cross flow plane, the CLVs exhibit the largest w_{rms} for both the ILES and experiment. Together with the reduction of circulation as shown in Fig. 10 it indicates the accelerated dissipation process compared to the WLVs. As the vortex system moves further downstream the turbulence inside the WLV increases faster for the experiment as it does in the ILES. Peak turbulence intensities exhibit a level of 3.5 % at x* = 4.0 increasing up to a level of approximately 6 % (experiment) and 5 % (ILES), respectively. While the CLV is nearly completely dissipated in the experiment at x* = 16.0, it still has an influence on the turbulence structures in the ILES.

The comparison of the experiment and the numerical results demonstrate that the ILES computations, initialized with near field experimental quantities, predict very well the wake vortex development in the near field and the upstream mid field. Vortex positions as well as mean velocities and turbulence intensities are up to a certain extent in good agreement with the wind tunnel reference data. For further improvement wall boundary layers will be considered by means of wall models. Based on this study ILES computations will be carried out to predict the wake vortex development up to a distance of 50 spans downstream.

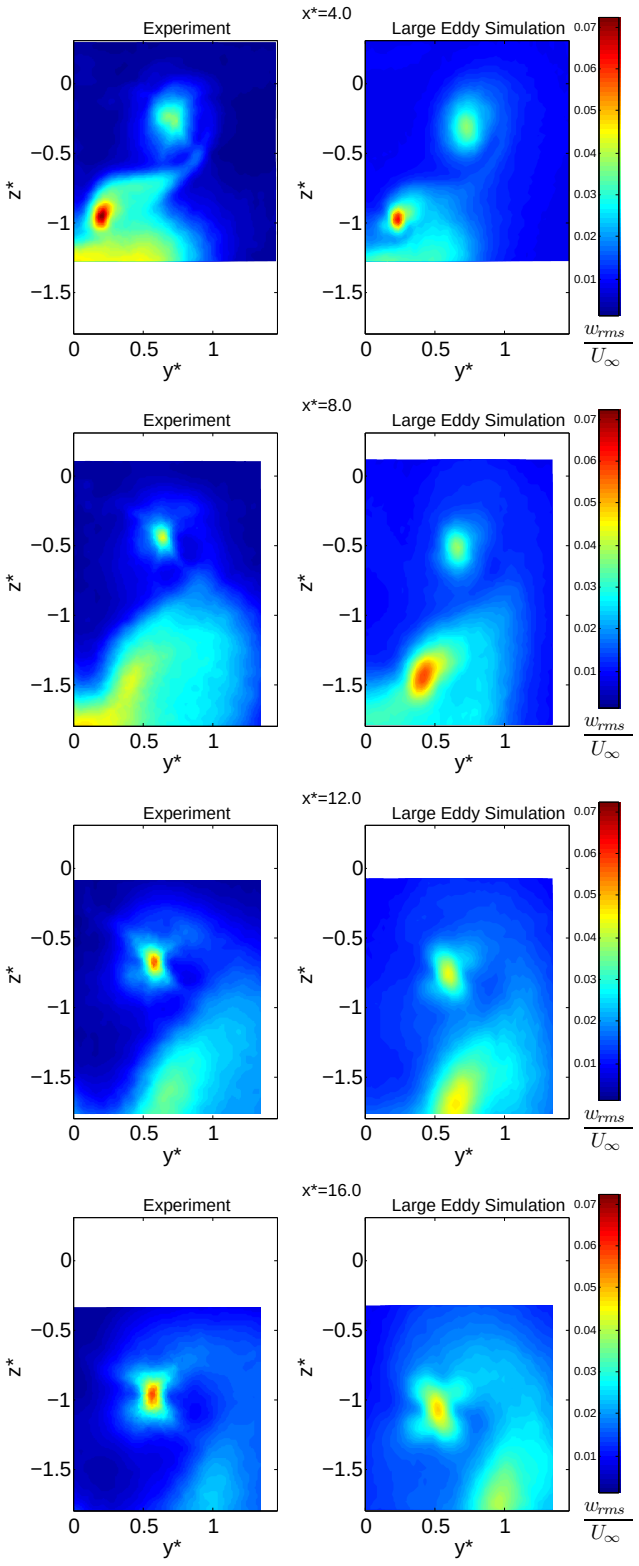

Fig. 15 Contour plots of nondimensional vertical turbulence intensity w_{rms}/U_∞ at x* = 4.0, 8.0, 12.0, and 16.0 for $Re_{l_\mu} = 5x10^5$ and $\alpha = 8$ deg

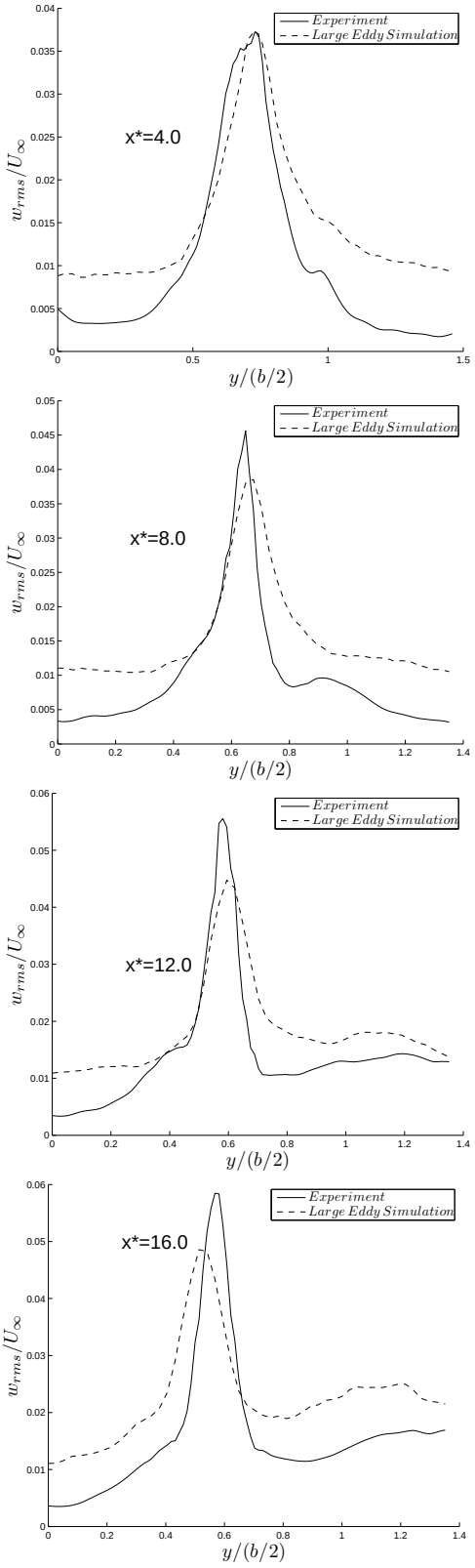

Fig. 16 Nondimensional vertical turbulence intensity w_{rms}/U_∞ along a horizontal cut through the vortex center for $Re_{l_\mu} = 5x10^5$ and $\alpha = 8$ deg

5 Conclusions and Outlook

The performed investigations determine the velocity distribution in the wake vortex system of a high-agility aircraft experimentally and numerically. The numerical approach is based on Implicit Large Eddy Simulations with the experimental data providing the initial and reference conditions. Using hot-wire anemometry the wake vortex system is investigated from the near field up to the mid field. The conducted validation calculations match well with the data of the experimental investigations. That makes ILES a suitable tool to predict the wake vortex system far downstream of the generating aircraft. Except small differences in the absolute values of the mean and turbulent velocity distributions, the spatial development of the wake vortex system is covered well. That can lead to the definition of flight areas behind a preceding aircraft which should be dodged by a following aircraft. This way critical unsteady loads due to the wake could be avoided. The results may also contribute to consider the associated loads during the design process. That counts for the discrete wake problem and for the continuous wake problem.

Literatur

[1] Luber W., Wake penetration effects on the dynamic loads and structural design of military and civil aircraft, IFASD, Seattle, June 2009.

[2] Breitsamter C., Nachlaufwirbelsysteme großer Transportflugzeuge, Habilitation, Technische Universität München, Herbert Utz Verlag Wissenschaft, ISBN 978-3-8316-0713-6, 2007.

[3] Donaldson C. duP, and Bilanin A. J., Vortex wakes of conventional aircraft, Technical Report AG-204, AGARD, 1975.

[4] Hünecke K., Structure of a Transport Aircraft-Type Near Field Wake, In: The Characterisation and Modification of Wakes from Lifting Vehicles in Fluids (Trondheim, Norway), May 1996, pp. 5-1-5-9 (AGARD-CP-584).

[5] Spalart, P. R., Airplane Trailing Vortices, Annual Review of Fluid Mechanics, Vol. 30, 1998, pp.107-138.

[6] Rossow V. J., Lift-Generated Vortex Wakes of Subsonic Transport Aircraft, Progress in Aerospace Sciences, Vol. 35, No. 6, 1999, pp. 507-560.

[7] Gerz, T. Holzäpfel, F. and Darracq, D., Commercial Aircraft Wake Vortices, Progress in Aerospace Sciences, Vol. 38, No. 3, 2002, pp. 181-208.

[8] Bisplinghoff R., Ashley H., Halfman R. L., Aeroelasticity, Dover Publications, Mineola, New York, 1996.

[9] Giesing J. P., Rodden W. P., and Stahl B., Sears Function and Lifting Surface Theory for Harmonic Gust Fields, Journal of Aircraft, Vol. 7, No. 3, pp. 252-255, 1970.

[10] Military Specification, Aircraft Strength and Rigidity, Flight Loads, MIL-A-008861A (USAF), March 1971.

[11] Grimaldi J. P., Britt, R. T. and Rodden W. P., Response of B-2 Aircraft to Nonuniform Spanwise Turbulence, Journal of Aircraft, Vol. 30, No. 5, pp. 652-659, 1993.

[12] Wright J. R., Cooper J. E., Introduction to Aircraft Aeroelasticity and Loads, Published by John Wiley and Sons, ISBN 1-56347-935-4 2008.

[13] Breitsamter C., Unsteady Aerodynamics, Lecture manuscript, Institute of Aerodynamics, Technische Universität München, 2009.

[14] Iatrou M., Allen, A. Pechloff A., Breitsamter C., and Laschka, B., Small Disturbance Euler-/Navier-Stokes Computations for Delta Wing Flap Oscillations. In: Flow Induced Unsteady Loads and the Impact on Military Applications, RTO-MP-AVT-123, Paper 16, Budapest, Hungary, April 25 - 28, 2005, pp. 16-1- 16-20.

[15] Hickel S., Implicit Turbulence Modeling for Large-Eddy Simulation, Dissertation, Technische Universität München, June 2008.

[16] Bruun H. H., Hot-Wire Anemometry, Oxford Science Publications, ISBN 0-19856342-6, 1995.

[17] Breitsamter C., Turbulente Strömungsstrukturen an Flugzeugkonfigurationen mit Vorderkantenwirbelsystemen, Dissertation, DM 18432, Technische Universität München, Verlag Wissenschaft (Aerodynamik), Germany, ISBN 3-89675-201-4, June 1997.

[18] Schlichting H., Truckenbrodt E., Aerodynamik des Flugzeugs, Springer Verlag, 1960.

Contact Author Email Address

jan-ulrich.klar@aer.mw.tum.de

Copyright Statement